Commun. Comput. Phys.
doi: 10.4208/cicp.230815.090516a

Vol. **21**, No. 2, pp. 401-422
February 2017

An Online Generalized Multiscale Discontinuous Galerkin Method (GMsDGM) for Flows in Heterogeneous Media

Eric T. Chung[1,*], Yalchin Efendiev[2,3] and Wing Tat Leung[2]

[1] *Department of Mathematics, The Chinese University of Hong Kong, Hong Kong.*
[2] *Department of Mathematics, Texas A&M University, College Station, TX 77843-3368, USA.*
[3] *Numerical Porous Media SRI Center, King Abdullah University of Science and Technology (KAUST), Thuwal 23955-6900, Kingdom of Saudi Arabia.*

Received 23 August 2015; Accepted (in revised version) 9 May 2016

Abstract. Offline computation is an essential component in most multiscale model reduction techniques. However, there are multiscale problems in which offline procedure is insufficient to give accurate representations of solutions, due to the fact that offline computations are typically performed locally and global information is missing in these offline information. To tackle this difficulty, we develop an online local adaptivity technique for local multiscale model reduction problems. We design new online basis functions within Discontinuous Galerkin method based on local residuals and some optimally estimates. The resulting basis functions are able to capture the solution efficiently and accurately, and are added to the approximation iteratively. Moreover, we show that the iterative procedure is convergent with a rate independent of physical scales if the initial space is chosen carefully. Our analysis also gives a guideline on how to choose the initial space. We present some numerical examples to show the performance of the proposed method.

AMS subject classifications: 65N12, 65N30

Key words: Multiscale method, discontinuous Galerkin method, online basis functions, heterogeneous media.

1 Introduction

In this paper, we develop an online local adaptivity technique for a class of multiscale model reduction problems. Many realistic applications involve solving problems that contain multiple scales and high contrast. Direct solution methods for these problems

*Corresponding author. *Email addresses:* tschung@math.cuhk.edu.hk (E. T. Chung), efendiev@math.tamu.edu (Y. Efendiev), leungwt@math.tamu.edu (W. T. Leung)

 ©2017 Global-Science Press

https://doi.org/10.4208/cicp.230815.090516a Published online by Cambridge University Press

require fine-grid discretizations and result in large discrete systems that are computationally intractable. Common model reduction techniques perform the discretization of the problems on a coarse grid, which is much larger than the scales under consideration, with the aim of getting more efficient solution strategies. There are a variety of multiscale model reduction techniques based on numerical upscaling (e.g., [15,28,39]) or multiscale methods (e.g., [3,6–8,10,12,16,22–24,29]). Most of the existing techniques are based on the so called offline construction. In particular, reduced models are computed in a pre-processing step, called offline stage, before the actual simulations, called online stage, are performed. For instances, some effective media are pre-computed for methods based on numerical upscaling and some multiscale basis functions are pre-computed for multiscale finite element methods. While these methods are effective in a wide variety of applications, there are still situations for which these methods are inadequate to give reliable solutions unless a large dimensional offline space is employed. Some of these situations involve external source effects and distant effects, which are ignored by most multiscale model reduction methods since they are typically based on local constructions. Therefore, it is evident that offline procedures are sometimes not enough to give efficient reduced models. Hence, it is the purpose of this paper to design a novel multiscale model reduction method. Our proposed method is based on a combination of offline technique and an online enrichment technique. The online technique is able to produce a reduced model taking care of external sources and distant effects, without using global models. The online construction is also performed locally and adaptively in regions with more heterogeneities, giving very efficient reduced models.

Our proposed method follows the overall idea of the Generalized Multiscale Finite Element Method (GMsFEM), which is introduced in [18] and is a generalization of the classical multiscale finite element method [31] in the way that the coarse spaces are systematically enriched, taking into account small scale information and complex input spaces. Instead of conforming finite element spaces as in [18,31], we will use in this paper discontinuous Galerkin finite element spaces, which have some essential advantages (see [10,19]) in multiscale simulations because it allows coupling discontinuous basis functions. The discretization starts with a coarse grid and a space of snapshot functions, which are defined on coarse elements. A space reduction is then performed to obtain a much smaller offline space by means of spectral decomposition. The spectral decomposition is performed locally on coarse elements, thus the functions in the offline space are in general discontinuous across coarse edges. The offline space is used as the approximation space for the interior penalty discontinuous Galerkin (IPDG) discretization on the coarse grid for the problem under consideration, giving our generalized multiscale discontinuous Galerkin method (GMsDGM). We remark that the offline space is computed only once in the pre-processing offline stage, and the same set of basis functions is used for any given source terms and boundary conditions. A-priori error estimate can be derived as in [10,21,22] showing that the error is inverse proportional to the first eigenvalue corresponding to the first eigenfunction that is not used in the construction of the reduced space. Since the aim of the paper is the new online locally adaptive procedure

https://doi.org/10.4208/cicp.230815.090516a Published online by Cambridge University Press

and its convergence, we will not discuss a-priori error estimate in this paper. We remark that a heterogeneous multiscale DG method is analyzed for a class of problems with scale separation [1], and a class of variational multiscale methods using the DG formulation are analyzed in [25,26,33].

The previous paragraph discusses the offline component of our method. As we discussed before, some new basis functions are necessary to capture certain behavior of the solution which cannot be captured by offline basis functions. For example, the solution may contain heterogeneities due to some distant effects and source terms, and these cannot be incorporated efficiently by offline basis functions before the solution is computed. Hence, it is the purpose of this paper to develop a technique to find new basis functions in the online stage. Our method consists of an iterative procedure. Given an approximate solution, some local residuals on coarse elements can be computed to reflect the amount of error in these coarse elements. These local residuals serve as indicators to locate regions, where new online basis functions are necessary. We will show that the projection of these residuals to the fine-grid can be used as new basis functions and that the energy-norm error has the most decay in a certain sense when these residual-based basis functions are included in the next solution process. In addition, we will show that this iterative procedure is convergent with a convergence rate independent of scales and contrast. In our analysis of convergence, we will show that it is essential to choose the appropriate space to begin the iterative procedure (cf. [17,20,27]). This initial space is computed in the offline stage and is obtained from a carefully design spectral problem. With this choice of the initial space, we show that one can obtain a very fast decay of errors by adding our online basis functions. Finally, we remark that there are offline adaptive enrichment strategies in the context of GMsFEM. In particular, in [11], offline adaptive procedure is developed and its convergence is analyzed using techniques in [4,34]. This is an efficient method to adaptively enrich the offline space and is desirable for problems, where offline basis functions are good enough to capture the solution. On the other hand, we remark that other offline-based adaptive methods are available [2,5,13,14,25,30,32,35,38]. Also, we remark that online basis functions within continuous Galerkin GMsFEM is studied in [9], and that an online procedure for some parameter dependent problems is studied in [36].

The rest of the paper is organized in the following way. In the next section, we present the basic idea of GMsDGM and our online locally adaptive procedure. The method is then detailed and analyzed in Section 3. In Section 4, numerical results are illustrated to test the performance of this adaptive algorithm. Finally a conclusion is given in Section 5.

2 Preliminaries

In this paper, we consider the following high-contrast flow problem

$$-\text{div}\left(\kappa(x)\nabla u\right)=f \quad \text{in } D, \tag{2.1}$$

https://doi.org/10.4208/cicp.230815.090516a Published online by Cambridge University Press

subject to the homogeneous Dirichlet boundary condition $u=g$ on ∂D, where D is the computational domain and $f(x)$ is a given source term. We assume that the coefficient $\kappa(x)$ is highly heterogeneous with very high contrast. For the convenience of our analysis, we also assume that $\kappa(x)$ is bounded below, that is, $\kappa(x)\geq 1$. Due to the heterogeneity and high contrast of $\kappa(x)$, very fine meshes are necessary to obtain accurate numerical solutions. It is therefore crucial to develop a numerical scheme with a low dimensional approximation space for the efficient approximation of (2.1).

Next, we present some notations needed for the constructions of our scheme. Consider a given triangulation $\mathcal{T}^H$ of the domain D with mesh size $H>0$. For convenience, we assume the domain D is rectangular and that the triangulation $\mathcal{T}^H$ consists of rectangles. We call $\mathcal{T}^H$ the coarse grid and H the coarse mesh size. Elements of $\mathcal{T}^H$ are called coarse grid blocks and we use N to denote the number of coarse grid blocks. The set of all coarse grid edges is denoted by $\mathcal{E}^H$. See Fig. 1 for an illustration. We also introduce a finer triangulation $\mathcal{T}^h$ of the computational domain D, obtained by a conforming refinement of the coarse grid $\mathcal{T}^H$. We call $\mathcal{T}^h$ the fine grid and $h>0$ the fine mesh size.

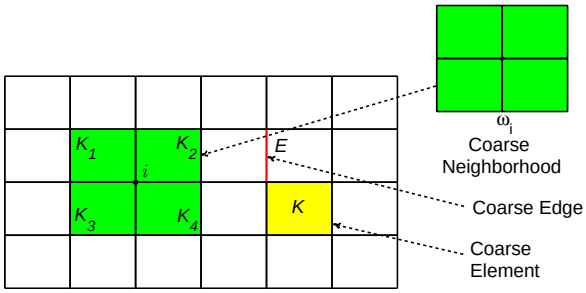


Figure 1: Illustration of a coarse neighborhood and a coarse element.

Now we present the framework of our GMsDGM. The methodology consists of two main ingredients, namely, the construction of local basis functions and the global coarse grid level coupling. For the coarse grid level coupling, we will apply the interior penalty discontinuous Galerkin (IPDG) method [37]. We remark that other discretizations can also be used. Assume that V_H is a given approximation space defined on the coarse grid $\mathcal{T}^H$. Functions in V_H are piecewise polynomials within coarse grid blocks and are in general discontinuous across coarse grid edges. Following standard procedures, the IPDG method reads: find $u_H\in V_H$ such that

$$a_{\mathrm{DG}}(u_H,v)=(f,v),\quad \forall v\in V_H, \tag{2.2}$$

where the bilinear form a_{DG} is defined as

$$a_{\mathrm{DG}}(u,v)=a_H(u,v)-\sum_{E\in\mathcal{E}^H}\int_E\Big(\{\{\kappa\nabla u\cdot n_E\}\}[[v]]+\{\{\kappa\nabla v\cdot n_E\}\}[[u]]\Big)+\sum_{E\in\mathcal{E}^H}\frac{\gamma}{h}\int_E\overline{\kappa}[[u]][[v]] \tag{2.3}$$

https://doi.org/10.4208/cicp.230815.090516a Published online by Cambridge University Press

with

$$a_H(u,v)=\sum_{K\in\mathcal{T}_H} a_H^K(u,v), \quad a_H^K(u,v)=\int_K \kappa\nabla u\cdot\nabla v, \tag{2.4}$$

where $\gamma>0$ is a penalty parameter, n_E is a fixed unit normal vector defined on the coarse edge $E\in\mathcal{E}^H$. Note that, in (2.3), the average and the jump operators are defined in the classical way. Specifically, consider an interior coarse edge $E\in\mathcal{E}^H$ and let K^+ and K^- be the two coarse grid blocks sharing the edge E. For a piecewise smooth function G with respect to the coarse grid $\mathcal{T}^H$, we define

$$\{\{G\}\}=\frac{1}{2}(G^++G^-), \qquad [[G]]=G^+-G^-, \qquad \text{on } E,$$

where $G^+=G|_{K^+}$ and $G^-=G|_{K^-}$ and we assume that the normal vector n_E is pointing from K^+ to K^-. Moreover, on the edge E, we define $\overline{\kappa}=(\kappa_{K^+}+\kappa_{K^-})/2$, where $\kappa_{K^\pm}$ is the maximum value of κ over $K^\pm$. For a coarse edge E lying on the boundary ∂D, we define

$$\{\{G\}\}=[[G]]=G, \quad \text{and} \quad \overline{\kappa}=\kappa_K \qquad \text{on } E,$$

where we always assume that n_E is pointing outside of D.

For our analysis, we define the DG-norm as

$$\|u\|_{\mathrm{DG}}^2=a_H(u,u)+\sum_{E\in\mathcal{E}^H}\frac{\gamma}{h}\int_E\overline{\kappa}[[u]]^2.$$

Then, the following continuity and coercivity of the bilinear form a_{DG} hold. We refer to [10] for the proof.

Lemma 2.1. *Assume that the penalty parameter γ is chosen so that $\gamma>C_{\mathrm{inv}}^2$. The bilinear form a_{DG} defined in (2.3) is continuous and coercive with respect to the DG-norm, that is,*

$$a_{DG}(u,v)\le a_1\|u\|_{DG}\|v\|_{DG}, \tag{2.5}$$

$$a_{DG}(u,u)\ge a_0\|u\|_{DG}^2, \tag{2.6}$$

for all $u,v\in V_H$, where $a_0=1-C_{\mathrm{inv}}\gamma^{-\frac{1}{2}}>0$ and $a_1=1+C_{\mathrm{inv}}\gamma^{-\frac{1}{2}}$.

One main result of the paper is a convergence estimate of an adaptive procedure for the problem (2.2). For this purpose, we will compare the multiscale solution u_H to a fine-scale solution u_h defined in the following way. We first let

$$V_{\mathrm{DG}}^h=\{v\in L^2(D): v|_K\in V^h(K)\},$$

where $V^h(K)$ is the space of continuous piecewise bilinear functions defined on K with respect to the fine grid. The fine-scale solution $u_h\in V_{\mathrm{DG}}^h$ is defined as the solution of the following

$$a_{\mathrm{DG}}(u_h,v)=(f,v), \quad \forall v\in V_{\mathrm{DG}}^h. \tag{2.7}$$

https://doi.org/10.4208/cicp.230815.090516a Published online by Cambridge University Press

It is well-known that u_h gives a good approximation to the exact solution u up to a coarse grid discretization error.

The second main component of our method is the construction of local basis functions, which contains two stages, namely the offline stage and the online stage. In the offline stage, a snapshot space $V^{i,\text{snap}}$ is first constructed for each coarse grid block $K_i \in \mathcal{T}^H$. The snapshot space contains a rich space of basis functions, which can be used to approximate the fine-scale solution defined (2.7) with a good accuracy. A spectral problem is then solved in the snapshot space $V^{i,\text{snap}}$ and eigenfunctions corresponding to dominant modes are used as the basis functions. The resulting space is called the local offline space $V^{i,\text{off}}$ for the i-th coarse grid block K_i. The global offline space V^{off} is then defined as the linear span of all these $V^{i,\text{off}}$, for $i=1,2,\cdots,N$. This global offline space V^{off} will be used as the initial space of our method. We denote this initial space as $V_H^{(0)}$. Using the initial space, an initial solution $u_H^{(0)}$ can be computed by solving (2.2). Local residuals in coarse grid blocks can then be computed based on the initial solution $u_H^{(0)}$. In coarse grid blocks with large residuals, new basis functions are computed and added to the approximation space. This procedure is continued until certain tolerance is reached. Next, we present a general outline of the method.

Assume that the initial space $V_H^{(0)}$ is given and the initial solution $u_H^{(0)}$ is computed. For any $m \geq 0$, we repeat the following until the solution $u_H^{(m)}$ satisfies certain tolerance requirement.

Step 1: Solve (2.2) using the space $V_H^{(m)}$ to obtain the solution $u_H^{(m)} \in V_H^{(m)}$.

Step 2: Compute local residuals based on the solution $u_H^{(m)}$.

Step 3: Construct new basis functions in regions, where the residuals are large.

Step 4: Add these basis functions to $V_H^{(m)}$ to form a new space $V^{(m+1)}$.

In the following, we will give the details of Step 2 and Step 3. We will also explain how one chooses the initial space $V_H^{(0)}$.

3 Locally online adaptivity

In this section, we will give details of our locally online adaptivity for the problem (2.2). As presented in the general outline of the method from the previous section, our adaptivity idea contains the choice of initial space as well as construction of new local multiscale basis functions. In the following, we will give the construction of these in detail.

3.1 Initial space

We present the definition of the initial space $V_H^{(0)}$. Let x_i be a node in the coarse grid $\mathcal{T}^H$, referred to as the i-th coarse node, for $i=1,2,\cdots,N_c$, where N_c is the number of nodes in

https://doi.org/10.4208/cicp.230815.090516a Published online by Cambridge University Press

the coarse grid $\mathcal{T}^H$. We will then define the i-th coarse neighbourhood ω_i as the union of all coarse grid blocks having the node x_i, see Fig. 1. Moreover, for each coarse grid block $K\in\mathcal{T}^H$, we let $\chi^K_{(j)}$, $j=1,2,3,4$, be the partition of unity functions, having value 1 at one vertex y_j and value 0 at the remaining three vertices, where y_j, $j=1,2,3,4$, are the four vertices of K. Note that there is exactly one value of j such that the vertex y_j is the same as the vertex x_i. In the case, we write $\chi^K_{(j)}=\chi^K_i$. One can use the standard multiscale basis functions or bilinear functions as the partition of unity functions. Note that we do not require any continuity of these partition of unity functions across coarse grid edges. The partition of unity functions are all supported on coarse grid blocks. Furthermore, we define the space $V^h(\omega_i)$ by

$$V^h(\omega_i)=\{v\in L^2(\omega_i): v|_K\in V^h(K), K\in\mathcal{T}^H, K\subset\omega_i\},$$

where $V^h(K)$ is the space of continuous piecewise bilinear functions defined on K. We remark that functions in $V^h(\omega_i)$ are supported in ω_i and belong to the space $V^h(K)$ for each coarse grid block $K\subset\omega_i$. Note that there is no continuity condition across boundaries of coarse grid blocks. We consider $V^h(\omega_i)$ as the snapshot space in ω_i, that is $V^{i,\text{snap}}=V^h(\omega_i)$, and perform a dimension reduction through a spectral problem. For this purpose, we define $\mathcal{E}^H_i$ be the set of coarse grid edges lying in the interior of ω_i, and the following bilinear form

$$a_{\omega_i}(u,v)=\sum_{K\in\mathcal{T}^H,K\subset\omega_i}a^K_H(u,v)+\sum_{E\in\mathcal{E}^H_i}\frac{\gamma}{h}\int_E\overline{\kappa}[[u]][[v]],\quad\forall u,v\in V^h(\omega_i).\tag{3.1}$$

Based on our analysis to be presented next, we solve the following spectral problem

$$a_{\omega_i}(u,v)=\lambda s_{\omega_i}(u,v),\quad\forall v\in V^h(\omega_i),\tag{3.2}$$

where

$$s_{\omega_i}(u,v)=\sum_{K\in\mathcal{T}^H,K\subset\omega_i}\int_K\kappa|\nabla\chi^K_i|^2uv+\sum_{E\in\mathcal{E}^H_i}\frac{\gamma}{h}\int_E\overline{\kappa}[[\chi^K_i]]^2\{\{u\}\}\{\{v\}\},\quad\forall u,v\in V^h(\omega_i).\tag{3.3}$$

We use the notations $\lambda^{\omega_i}_k$ and $\Psi^{\omega_i}_k$ to denote the k-th eigenvalue and the k-th eigenvector of the above spectral problem (3.2). Each eigenfunction $\Psi^{\omega_i}_k$ corresponds to a function in $\psi^{\omega_i}_k\in V^h(\omega_i)$ defined by

$$\psi^{\omega_i}_k=\sum_{j=1}^{n_i}(\Psi^{\omega_i}_k)_j w^{\omega_i}_j,\tag{3.4}$$

where n_i is the dimension of $V^h(\omega_i)$ and $\{w^{\omega_i}_j\}_{j=1}^{n_i}$ is a basis for $V^h(\omega_i)$. In the above definition, $(\Psi^{\omega_i}_k)_j$ is the j-th component of the eigenvector $\Psi^{\omega_i}_k$.

For each ω_i, we solve the spectral problem (3.2) and the first L_i eigenfunctions are used to form the initial space. Each eigenfunction $\psi^{\omega_i}_k$ will be first multiplied by the partition of unity function χ^K_i, for each $K\subset\omega_i$, and is then decoupled across coarse grid edges

https://doi.org/10.4208/cicp.230815.090516a Published online by Cambridge University Press

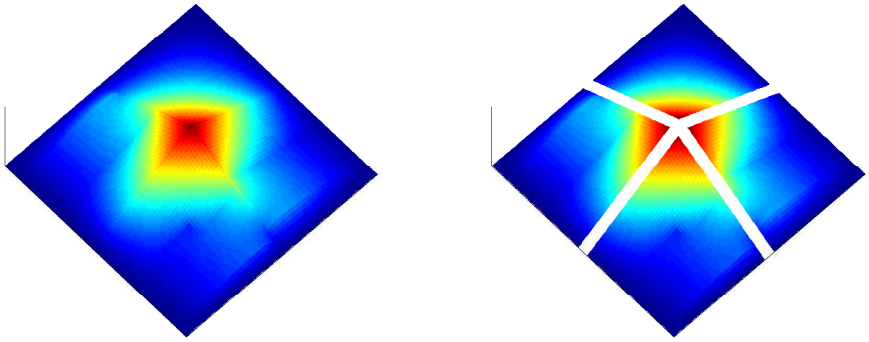


Figure 2: Illustration of the initial basis construction. Left: An eigenfunction $\chi_i^K\psi_k^{\omega_i}$ is defined in ω_i. Right: 4 basis functions are obtained by splitting $\chi_i^K\psi_k^{\omega_i}$ into 4 pieces, and each has support in $K\subset\omega_i$.

to form 4 basis functions. In particular, the 4 new basis functions have support in one of the coarse grid block forming ω_i and are zero in the other three coarse grid blocks forming ω_i. For example, if $K\subset\omega_i$, the basis function is $\chi_i^K\psi_k^{\omega_i}$. We write $V^{i,\text{off}}$ as the space spanned by $I_K(\chi_i^K\psi_k^{\omega_i})$, for all $K\subset\omega_i$, where I_K is the standard bilinear interpolation operator. Therefore, $V^{i,\text{off}}$ is a subspace of V^h. See Fig. 2 for an illustration. The initial space $V_H^{(0)}$ is obtained by the linear span of all functions constructed in the above procedure. Notice that $V_H^{(0)}\subset V_{\text{DG}}^h$.

3.2 Construction of online basis functions

In this section, we will discuss the construction of our local online basis functions. The purpose is to add basis functions locally in some coarse neighborhoods to obtain rapidly decaying errors. Assume that the space $V_H^{(m)}$ at the m-th iteration and the corresponding solution $u_H^{(m)}$ are given. For each coarse neighborhood ω_i, we define the local residual by

$$R_i^{(m)}(v)=(f,v)-a_{\text{DG}}(u_H^{(m)},v),\quad v\in V_0^h(\omega_i), \tag{3.5}$$

where $V_0^h(\omega_i)\subset V^h(\omega_i)$ contains functions that are zero on $\partial\omega_i$ and

$$V^h(\omega_i)=\{v\in L^2(\omega_i):v|_K\in V^h(K),K\in\mathcal{T}^H,K\subset\omega_i\}.$$

The residual $R_i^{(m)}$ can be seen as a linear functional defined on $V_0^h(\omega_i)$ with norm $\|R_i^{(m)}\|$ defined by

$$\|R_i^{(m)}\|=\sup_{v\in V_0^h(\omega_i)}\frac{|R_i^{(m)}(v)|}{\|v\|_{\omega_i}}, \tag{3.6}$$

https://doi.org/10.4208/cicp.230815.090516a Published online by Cambridge University Press

and $\|v\|^2_{\omega_i}=a_{\omega_i}(v,v)$. We will then find the new online basis function $\phi\in V_0^h(\omega_i)$ by solving

$$a_{\omega_i}(\phi,v)=R_i^{(m)}(v),\quad \forall v\in V_0^h(\omega_i). \tag{3.7}$$

The new online basis function ϕ is added to $V_H^{(m)}$ to form $V_H^{(m+1)}$.

The motivation of finding a new basis function ϕ by solving (3.7) can be explained as follows. We define the A-norm by

$$\|u\|_A^2=a_{\mathrm{DG}}(u,u),\quad \forall u\in V_H.$$

We notice that the A-norm is equivalent to the DG-norm $\|u\|_{\mathrm{DG}}$ by Lemma 2.1. From (2.2) and (2.7), we have the following Galerkin orthogonality condition

$$a_{\mathrm{DG}}(u_h-u_H^{(m)},v)=0,\quad \forall v\in V_H^{(m)}. \tag{3.8}$$

Thus, we see that the following optimal error bound holds

$$\|u_h-u_H^{(m)}\|_A^2\leq\|u_h-\widetilde{u}\|_A^2,\quad \forall\widetilde{u}\in V_H^{(m)}. \tag{3.9}$$

Notice that (3.8) and (3.9) hold for any $m\geq 0$.

We will enrich the space $V_H^{(m)}$ by adding a basis function ϕ in the space $V_0^h(\omega_i)$ to form $V_H^{(m+1)}$. First, (3.9) implies

$$\|u_h-u_H^{(m+1)}\|_A^2\leq\|u_h-\widetilde{u}\|_A^2,\quad \forall\widetilde{u}\in V_H^{(m+1)}. \tag{3.10}$$

Taking $\widetilde{u}=u_H^{(m)}+\alpha\phi$, for some scalar α, in (3.10), we have

$$\|u_h-u_H^{(m+1)}\|_A^2\leq\|u_h-u_H^{(m)}-\alpha\phi\|_A^2$$

which implies

$$\|u_h-u_H^{(m+1)}\|_A^2\leq\|u_h-u_H^{(m)}\|_A^2-2\alpha a_{\mathrm{DG}}(u_h-u_H^{(m)},\phi)+\alpha^2\|\phi\|_A^2.$$

Taking $\alpha=a_{\mathrm{DG}}(u_h-u_H^{(m)},\phi)/\|\phi\|_A^2$, we obtain

$$\|u_h-u_H^{(m+1)}\|_A^2\leq\|u_h-u_H^{(m)}\|_A^2-\frac{a_{\mathrm{DG}}(u_h-u_H^{(m)},\phi)^2}{\|\phi\|_A^2}. \tag{3.11}$$

By the definition of the residual $R_i^{(m)}$ in (3.5), we see that (3.11) becomes

$$\|u_h-u_H^{(m+1)}\|_A^2\leq\|u_h-u_H^{(m)}\|_A^2-\frac{(R_i^{(m)}(\phi))^2}{\|\phi\|_A^2}. \tag{3.12}$$

https://doi.org/10.4208/cicp.230815.090516a Published online by Cambridge University Press

From (3.12), we see that the quantity $(R_i^{(m)}(\phi))^2/\|\phi\|_A^2$ measures the amount of reduction in error when the basis function ϕ is added in $V_H^{(m)}$ to form $V_H^{(m+1)}$. We will construct the function $\phi\in V_0^h(\omega_i)$ to obtain the most reduction in error. Thus, we find $\phi\in V_0^h(\omega_i)$ that maximizes $R_i^{(m)}(\phi)/\|\phi\|_A$. Equivalently, we find $\phi\in V_0^h(\omega_i)$ by solving

$$a_{\omega_i}(\phi,v)=R_i^{(m)}(v),\quad \forall v\in V_0^h(\omega_i).$$

Notice that, we have used the fact that $\|\phi\|_A=\|\phi\|_{\omega_i}$ when $\phi\in V_0^h(\omega_i)$.

Next, we summarize our online GMsDGM:

- *Initialization:* We will construct the initial space $V_H^{(0)}$. For each coarse neighborhood ω_i, we solve the following spectral problem in the space $V^h(\omega_i)$:

  $$a_{\omega_i}(u,v)=\lambda s_{\omega_i}(u,v).$$

  Then we obtain the eigenfunctions $\psi_k^{\omega_i}$ by (3.4), and we will consider the restriction of $\psi_k^{\omega_i}$ in each coarse element in ω_i as an individual function. Using the first L_i of these eigenfunctions, we obtain the basis functions $I_K(\chi_i^L\psi_k^{\omega_i})$.

- *Iteration:* For each $m\geq 0$, we perform the following iterations.

  1. Find $u_H^{(m)}\in V_H^{(m)}$ by solving

     $$a_{\mathrm{DG}}(u_H^{(m)},v)=(f,v),\quad \forall v\in V_H^{(m)}.$$

  2. Choose non-overlapping coarse neighborhoods ω_i and find new basis functions $\phi\in V_0^h(\omega_i)$ by

     $$a_{\omega_i}(\phi,v)=R_i^{(m)}(v),\quad \forall v\in V_0^h(\omega_i).$$

  3. Add those basis functions to $V_H^{(m)}$ to form $V_H^{(m+1)}$.

3.3 Convergence of the adaptive procedure

In this section, we analyze the convergence of the above online enrichment procedure. Before proving the convergence, we need the following lemma which will can be proved by standard techniques.

Lemma 3.1. *There exists a positive constant C_I such that*

$$\|I(v)\|_{\mathrm{DG}}\leq C_I\|v\|_{\mathrm{DG}},\quad \forall v\in V_{DG}^h, \tag{3.13}$$

where $I(v)|_K=I_K(v)$ for all $K\in\mathcal{T}^H$.

https://doi.org/10.4208/cicp.230815.090516a Published online by Cambridge University Press

We begin the convergence analysis at the inequality (3.12). Notice that, this inequality can be written as

$$\|u_h - u_H^{(m+1)}\|_A^2 \leq \|u_h - u_H^{(m)}\|_A^2 - \|R_i^{(m)}\|^2, \tag{3.14}$$

when the basis function ϕ is obtained as in (3.7).

On the other hand, we will show that the error $\|u_h - u_H^{(m)}\|_A$ can be controlled by the residual norm $\|R_i^{(m)}\|$. To do so, we consider an arbitrary function $v \in V_{\mathrm{DG}}^h$. Let $v_i \in V^h(\omega_i)$ be the restriction of v in ω_i, and let $v_i^{(0)} \in V^{i,\mathrm{off}}$ be the component of v_i in the offline space $V^{i,\mathrm{off}}$. By the GMsDGM (2.2), the fine-grid problem (2.7) and the Galerkin orthogonality (3.8), we have

$$a_{\mathrm{DG}}(u_h - u_H^{(m)}, v) = a_{\mathrm{DG}}(u_h - u_H^{(m)}, v - v^{(0)}), \quad \forall v^{(0)} \in V_H^{(0)},$$

where we define $v^{(0)} = \sum_{i=1}^{N_c} v_i^{(0)} \in V_H^{(0)}$ and use the fact that $V_H^{(0)} \subset V_H^{(m)}$ for all $m \geq 0$. By (2.7), we have

$$a_{\mathrm{DG}}(u_h - u_H^{(m)}, v) = (f, v - v^{(0)}) - a_{\mathrm{DG}}(u_H^{(m)}, v - v^{(0)}).$$

Using the property $\sum_{j=1}^{4} \chi_{(j)}^K = 1$ for all $K \in \mathcal{T}^H$ and the linearity of interpolation operator I,

$$a_{\mathrm{DG}}(u_h - u_H^{(m)}, v) = \sum_{K \in \mathcal{T}^H} \sum_{j=1}^{4} \Big((f, I_K(\chi_{(j)}^K (v - v_i^{(0)}))) - a_{\mathrm{DG}}(u_H^{(m)}, I_K(\chi_{(j)}^K (v - v_i^{(0)}))) \Big).$$

Writing the above sum over coarse neighborhoods ω_i, we have

$$a_{\mathrm{DG}}(u_h - u_H^{(m)}, v) = \sum_{i=1}^{N_c} \sum_{K \subset \omega_i} \Big((f, I_K(\chi_i^K (v - v_i^{(0)}))) - a_{\mathrm{DG}}(u_H^{(m)}, I_K(\chi_i^K (v - v_i^{(0)}))) \Big).$$

For each coarse neighborhood ω_i, we define the following modified local residual by

$$\widetilde{R}_i^{(m)}(v) = \sum_{K \subset \omega_i} \Big((f, I_K(\chi_i^K v)) - a_{\mathrm{DG}}(u_H^{(m)}, I_K(\chi_i^K v)) \Big), \quad v \in V^h(\omega_i). \tag{3.15}$$

The modified residual $\widetilde{R}_i^{(m)}$ can be seen as a linear functional defined on $V^h(\omega_i)$ with norm $\|\widetilde{R}_i^{(m)}\|$ defined in the following way

$$\|\widetilde{R}_i^{(m)}\| = \sup_{v \in V^h(\omega_i)} \frac{|\widetilde{R}_i^{(m)}(v)|}{\|\sum_{K \subset \omega_i} I_K(\chi_i^K v)\|_{\omega_i}}.$$

In the above definitions, χ_i^K is considered to be defined only on K, and has zero value outside K.

https://doi.org/10.4208/cicp.230815.090516a Published online by Cambridge University Press

Using the definition of the modified residual $\widetilde{R}_i^{(m)}$, we have

$$a_{\mathrm{DG}}(u_h-u_H^{(m)},v)\leq\sum_{i=1}^{N_c}\|\widetilde{R}_i^{(m)}\|\|\sum_{K\subset\omega_i}I_K(\chi_i^K(v-v_i^{(0)}))\|_A, \tag{3.16}$$

where we used the fact that $\sum_{K\subset\omega_i}I_K(\chi_i^K(v-v_i^{(0)}))$ is zero on $\partial\omega_i$. Using Lemma 2.1,

$$\|\sum_{K\subset\omega_i}I_K(\chi_i^K(v-v_i^{(0)}))\|_A\leq a_1^{\frac{1}{2}}\|\sum_{K\subset\omega_i}I_K(\chi_i^K(v-v_i^{(0)}))\|_{\mathrm{DG}}. \tag{3.17}$$

By the definition of the DG-norm and Lemma 3.1,

$$\begin{aligned}\|I_K(\chi_i^K(v-v_i^{(0)}))\|_{\mathrm{DG}}^2&\leq C_I^2\|\chi_i^K(v-v_i^{(0)})\|_{\mathrm{DG}}^2\\&=C_I^2\Big(\sum_{K\subset\omega_i}\int_K\kappa|\nabla(\chi_i^K(v-v_i^{(0)}))|^2+\frac{\gamma}{h}\sum_e\int_e\overline{\kappa}[[\chi_i^K(v-v_i^{(0)})]]^2\Big).\end{aligned} \tag{3.18}$$

For each $K\subset\omega_i$, we have

$$\int_K\kappa|\nabla(\chi_i^K(v-v_i^{(0)}))|^2\leq 2\int_K\kappa\chi_i^2|\nabla(v-v_i^{(0)})|^2+2\int_K\kappa|\nabla\chi_i^K|^2(v-v_i^{(0)})^2. \tag{3.19}$$

For each $e\in\mathcal{E}_i^H$, we have

$$\int_e\overline{\kappa}[[\chi_i^K(v-v_i^{(0)})]]^2\leq 2\int_e\overline{\kappa}\{\{\chi_i^K\}\}^2[[v-v_i^{(0)}]]^2+2\int_e\overline{\kappa}[[\chi_i^K]]^2\{\{v-v_i^{(0)}\}\}^2. \tag{3.20}$$

Combining inequalities (3.19) and (3.20) in (3.18), we have

$$\begin{aligned}&\|I_K(\chi_i^K(v-v_i^{(0)}))\|_{\mathrm{DG}}^2\\&\leq 2C_I^2\|v-v_i^{(0)}\|_{A_i}^2+2C_I^2\Big(\int_{\omega_i}\overline{\kappa}|\nabla\chi_i^K|^2(v-v_i^{(0)})^2+\frac{\gamma}{h}\sum_{e\in\mathcal{E}_i^H}\int_e\overline{\kappa}[[\chi_i^K]]^2\{\{v-v_i^{(0)}\}\}^2\Big),\end{aligned} \tag{3.21}$$

where $\|v\|_{A_i}^2=a_{\omega_i}(v,v)$. Using the spectral problem (3.2), we have

$$\|v-v_i^{(0)}\|_{A_i}^2=a_{\omega_i}(v_i-v_i^{(0)},v_i-v_i^{(0)})\leq a_{\omega_i}(v_i,v_i)=\|v\|_{A_i}^2$$

and

$$\int_{\omega_i}\overline{\kappa}|\nabla\chi_i^K|^2(v-v_i^{(0)})^2+\frac{\gamma}{h}\sum_{e\in\mathcal{E}_i^H}\int_e\overline{\kappa}[[\nabla\chi_i^K]]^2\{\{v-v_i^{(0)}\}\}^2=s_{\omega_i}(v_i-v_i^{(0)},v_i-v_i^{(0)})\leq\frac{1}{\lambda_{L_i+1}^{\omega_i}}\|v\|_{A_i}^2.$$

Thus, (3.21) and (3.17) implies

$$\|I_K(\chi_i^K(v-v_i^{(0)}))\|_A^2\leq 2a_1C_I^2\Big(1+\frac{1}{\lambda_{L_i+1}^{\omega_i}}\Big)\|v\|_{A_i}^2.$$

https://doi.org/10.4208/cicp.230815.090516a Published online by Cambridge University Press

Hence, (3.16) becomes

$$a_{\mathrm{DG}}(u_h-u_H^{(m)},v)\leq\Big(\sum_{i=1}^{N_c}2a_1C_I^2(1+\frac{1}{\lambda_{L_i+1}^{\omega_i}})\|\widetilde{R}_i^{(m)}\|^2\Big)^{\frac{1}{2}}\Big(\sum_{i=1}^{N_c}\|v\|_{A_i}^2\Big)^{\frac{1}{2}}.$$

We remark that the above inequality holds for any $v\in V_{\mathrm{DG}}^h$. Taking $v=v_h-v_H^{(m)}$ and using Lemma 2.1, we finally obtain

$$\|u_h-u_H^{(m)}\|_A^2\leq 2a_0^{-1}a_1C_0C_I^2\sum_{i=1}^{N_c}\Big(1+\frac{1}{\lambda_{L_i+1}^{\omega_i}}\Big)\|\widetilde{R}_i^{(m)}\|^2, \tag{3.22}$$

where $C_0=\max_{K\in\mathcal{T}^H}n_K$ and n_K is the number of vertices of the coarse grid block K.

We define

$$\theta=\|R_i^{(m)}\|^2/\eta^2,\quad\text{and}\quad\eta^2=2a_0^{-1}a_1C_0C_I^2\sum_{i=1}^{N_c}\Big(1+\frac{1}{\lambda_{L_i+1}^{\omega_i}}\Big)\|\widetilde{R}_i^{(m)}\|^2. \tag{3.23}$$

From (3.14) and (3.22), we see that the following convergence holds

$$\|u_h-u_H^{(m+1)}\|_A^2\leq(1-\theta)\|u_h-u_H^{(m)}\|_A^2.$$

We summarize the above results in the following theorem.

Theorem 3.1. *Let u_h be the solution of (2.7) and $u_H^{(m)}$, $m\geq 0$, be the solution of (2.2) in the m-th iteration. Then the following residual bound holds*

$$\|u_h-u_H^{(m)}\|_A^2\leq 2a_0^{-1}a_1C_0C_I^2\sum_{i=1}^{N_c}\Big(1+\frac{1}{\lambda_{L_i+1}^{\omega_i}}\Big)\|\widetilde{R}_i^{(m)}\|^2. \tag{3.24}$$

Moreover, the following convergence holds

$$\|u_h-u_H^{(m+1)}\|_A^2\leq(1-\theta)\|u_h-u_H^{(m)}\|_A^2, \tag{3.25}$$

where θ is defined in (3.23).

We remark that one can derive a priori error estimate for the error $\|u_h-u_H^{(m)}\|_{\mathrm{DG}}$, for every $m\geq 0$. Since the purpose of this paper is an a posteriori error estimate (3.24) and the convergence of an adaptive enrichment algorithm (3.25), we will not derive a priori error estimate.

Finally, we remark that by using more basis functions in the initial space $V_H^{(0)}$, the values of the eigenvalues $\lambda_{L_i+1}^{\omega_i}$ are larger. Thus, the value of θ is further away from zero, and this fact enhances the convergence rate. In particular, the convergence rate is affected by the quantity $\Lambda_{\min}=\min_{1\leq i\leq N_c}\lambda_{L_i+1}^{\omega_i}$. The convergence is slow when $\Lambda_{\min}$ is small (cf. [9, 27]). We also remark that one can add online basis functions in multiple

https://doi.org/10.4208/cicp.230815.090516a Published online by Cambridge University Press

coarse neighborhoods to speed up the convergence. Let S be the index set for which online basis functions are added in ω_i for $i \in S$. By using similar arguments as above, we obtain

$$\|u_h - u_H^{(m+1)}\|_A^2 \leq (1-\widetilde{\theta})\|u_h - u_H^{(m)}\|_A^2,$$

where

$$\widetilde{\theta} = \sum_{i \in S} \|R_i^{(m)}\|^2 / \eta^2.$$

4 Numerical results

In this section, we will present some numerical examples to show the performance of the proposed method. The implementation procedure of online adaptive GMsDGM is described below. First, we choose a fixed number of functions for every coarse neighborhood by solving the local spectral problem. This fixed number for every coarse neighborhood is called the number of initial basis. After that, we split these functions into the basis functions of the offline space such that each basis function is supported in one coarse grid block. We denote this offline space as V^{off} and set $V_H^{(0)} = V^{\text{off}}$.

The coarse neighborhoods are denoted by $\omega_{i,j}$, where $i = 1,2,\cdots,N_x$ and $j = 1,2,\cdots,N_y$ and N_x and N_y are the number of coarse nodes in the x and y directions respectively. We consider $I_{x,\text{odd}}$ and $I_{x,\text{even}}$ as the set of odd and even indices from $\{1,2,\cdots,N_x\}$. Similarly, $I_{y,\text{odd}}$ and $I_{y,\text{even}}$ are the set of odd and even indices from $\{1,2,\cdots,N_y\}$. In each iteration of our online adaptive GMsDGM, we will perform 4 sub-iterations which add online basis functions in the non-overlapping coarse neighborhoods $\omega_{i,j}$ with $(i,j) \in I_{x,\text{odd}} \times I_{y,\text{odd}}$, $(i,j) \in I_{x,\text{odd}} \times I_{y,\text{even}}$, $(i,j) \in I_{x,\text{even}} \times I_{y,\text{odd}}$ and $(i,j) \in I_{x,\text{even}} \times I_{y,\text{even}}$ respectively.

We will take $\gamma = 2$ and $D = [0,1]^2$. The domain is divided into 10×10 uniform square coarse blocks. Each coarse block is then divided into 10×10 fine blocks consisting of uniform squares. Namely, the whole domain is partitioned by 100×100 fine grid blocks. The medium parameter κ is shown in Fig. 3. The source function f is taken as the constant 1. To compare the accuracy, we will use the following error quantities

$$e_2 = \frac{\|u_h - u_H\|_{L^2(D)}}{\|u_h\|_{L^2(D)}}, \quad \text{and} \quad e_a = \frac{\|u_h - u_H\|_{\text{DG}}}{\|u_h\|_{\text{DG}}}.$$

4.1 Comparison of using different number of initial basis

In Table 1, we present the convergence history of our algorithm for using one, two, three, four initial basis per coarse neighborhood. Notice that, in the presentation of our results, DOF means the total number of basis functions used in the whole domain and m denotes the number of iterations. We use the continuous multiscale basis functions as the initial partition of unity. In the tables, we obtain a fast error decay which give us a numerical solution with error smaller than 0.1% in two or three iterations. We can see the error

https://doi.org/10.4208/cicp.230815.090516a Published online by Cambridge University Press

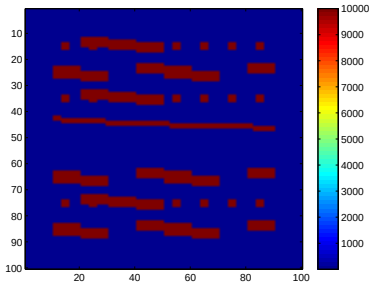


Figure 3: Permeability field κ.

Table 1: Top-left: One initial basis ($\Lambda_{\min}=4.89e-4$). Top-right: Two initial basis ($\Lambda_{\min}=0.9504$). Bottom-left: Three initial basis ($\Lambda_{\min}=1.4226$). Bottom-right: Four initial basis ($\Lambda_{\min}=2.2045$).

m	DOF	e_a	e_2
0	324	44.50%	24.88%
1	648	9.92%	2.18%
2	972	0.78%	7.54e-2%
3	1296	3.24e-2%	2.13e-3%
4	1620	2.42e-4%	1.10e-5%

m	DOF	e_a	e_2
0	648	17.73%	3.58%
1	972	0.31%	1.80e-2%
2	1296	3.52e-3%	1.62e-4%
3	1620	1.81e-5%	8.58e-7%
4	1948	1.04e-7%	4.68e-9%

m	DOF	e_a	e_2
0	972	11.30%	1.72%
1	1296	0.45%	2.44e-2%
2	1620	3.05e-3%	1.37e-4%
3	1944	1.06e-5%	4.08e-7%
4	2240	4.59e-8%	2.14e-9%

m	DOF	e_a	e_2
0	1296	8.38%	1.00%
1	1620	7.98e-2%	3.13e-3%
2	1944	9.93e-4%	3.57e-5%
3	2268	1.39e-5%	5.15e-7%
4	2540	4.23e-8%	1.55e-9%

decay of using one initial basis is slower than the error decay of using two or more initial basis since $\Lambda_{\min}$ for using one initial basis is too small.

To further study the importance of the initial basis, we will present another example with a different medium parameter κ shown in Fig. 4. The domain D is divided into

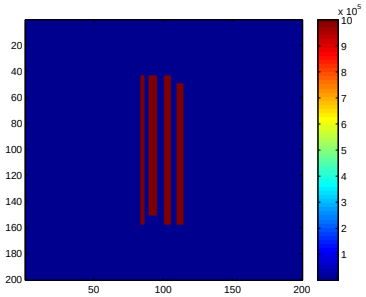


Figure 4: Permeability field κ.

https://doi.org/10.4208/cicp.230815.090516a Published online by Cambridge University Press

Table 2: One initial basis. Left: Lower contrast(1e4)($\Lambda_{\text{min}} = 0.0062$). Right: Higher contrast(1e6)($\Lambda_{\text{min}} = 6.22e-5$).

m	DOF	e_a	e_2
0	64	25.44%	6.67%
1	128	1.20%	0.23%
2	192	0.47%	0.10%
3	256	0.26%	5.79e-2%
4	320	0.10%	2.30e-2%
5	384	6.22e-2%	1.02e-2%
6	448	3.70e-4%	1.57e-5%

m	DOF	e_a	e_2
0	64	25.45%	6.67%
1	128	1.45%	0.27%
2	192	1.39%	0.27%
3	256	0.84%	0.15%
4	320	0.34%	7.98e-2%
5	384	0.34%	7.91e-2%
6	448	0.15%	3.71e-2%

Table 3: Two initial basis. Left: Lower contrast(1e4)($\Lambda_{\text{min}} = 0.027$). Right: Higher contrast(1e6)($\Lambda_{\text{min}} = 2.72e-4$).

m	DOF	e_a	e_2
0	128	18.22%	4.42%
1	192	1.14%	0.12%
2	256	0.50%	4.95e-2%
3	320	4.17e-2%	2.06e-3%
4	384	5.73e-3%	5.38e-4%
5	448	7.12e-4%	2.89e-5%

m	DOF	e_a	e_2
0	128	18.56%	4.62%
1	192	1.37%	0.16%
2	256	1.25%	0.14%
3	320	1.23%	0.13%
4	384	0.41%	3.22e-2%
5	448	3.63e-2%	3.56e-3%

Table 4: Three initial basis. Left: Lower contrast(1e4)($\Lambda_{\text{min}} = 0.0371$). Right: Higher contrast(1e6)($\Lambda_{\text{min}} = 3.75e-4$).

m	DOF	e_a	e_2
0	192	10.69%	1.86%
1	256	0.80%	6.66e-2%
2	320	0.34%	2.24e-2%
3	384	1.51e-2%	6.24e-4%
4	448	2.25e-4%	1.61e-5%
5	508	1.72e-6%	6.70e-8%

m	DOF	e_a	e_2
0	192	11.55%	2.14%
1	256	1.13%	0.10%
2	320	0.98%	8.85e-2%
3	384	0.96%	8.95e-2%
4	448	0.30%	1.39e-2%
5	508	2.00e-3%	8.39e-5%

5×5 coarse blocks consisting of uniform squares. Each coarse block is then divided into 40×40 fine blocks also consisting of uniform squares. The convergence history for the use of one, two, three, four initial basis and the corresponding total number of degrees of freedom (DOF) are shown in Table 2, Table 3, Table 4, Table 5 respectively. We consider two different contrasts. On the right table, we increase the contrast by 100 times. More precisely, the conductivity of inclusions and channels in Fig. 2 (left figure) is multiplied by 100. In this case, the first 4 eigenvalue that are in the regions with channels become 100 times smaller. The decrease in the eigenvalues will slow down the error decay. In Table 2, we can observe that the error decay for the lower contrast case is much faster than

https://doi.org/10.4208/cicp.230815.090516a Published online by Cambridge University Press

Table 5: Four initial basis. Left: Lower contrast(1e4)($\Lambda_{\min} = 0.4472$). Right: Higher contrast(1e6)($\Lambda_{\min} = 0.3844$).

m	DOF	e_a	e_2
0	248	7.92%	1.14%
1	312	0.25%	2.42e-2%
2	376	5.09e-3%	2.72e-4%
3	440	5.18e-5%	2.62e-6%
4	484	1.39e-6%	6.40e-8%

m	DOF	e_a	e_2
0	242	9.63%	1.59%
1	306	0.51%	5.40e-2%
2	370	1.38e-2%	9.46e-4%
3	434	2.10e-4%	1.59e-5%
4	494	1.74e-6%	1.27e-7%

the higher contrast case. In the higher contrast case, the error stop decreasing in some iterations. Similar observations are obtained when we use 2 or 3 initial basis. For using four initial basis, we observe a rapid convergence for both higher and lower contrast case.

4.2 Setting tolerance for the residual

In this section, we will show the performance for the online enrichment implementing it only for regions with a residual error bigger than a certain threshold. We consider the medium parameter shown in Fig. 3. We show the results for using three different tolerances (tol) 10^{-3}, 10^{-4} and 10^{-5}. We will enrich for the coarse regions with residual larger than the tolerance. In Table 6, we show the errors when using 1 initial basis function for tolerances 10^{-3}, 10^{-4} and 10^{-5}. We can see that the convergence history in the first few iteration is similar to the result shown in previous section. Moreover, the energy error of the multiscale solution is in the same order of the tolerance and the error will stop decreasing even if we perform more iterations. Therefore, we can compute a multiscale solution with a prescribed error level by choosing a suitable tolerance in the

Table 6: One initial basis. Left: $tol = 10^{-3}$. Middle: $tol = 10^{-4}$. Right: $tol = 10^{-5}$.

m	DOF	e_a	e_2
0	324	44.50%	24.88%
1	648	9.92%	2.18%
2	924	0.81%	7.72e-2%
3	976	0.29%	2.49e-2%

m	DOF	e_a	e_2
0	324	44.50%	24.88%
1	648	9.92%	2.18%
2	972	0.78%	7.54e-2%
3	1176	4.12e-2%	2.88e-3%
4	1184	2.65e-2%	1.57e-3%

m	DOF	e_a	e_2
0	324	44.50%	24.88%
1	648	9.92%	2.18%
2	972	0.78%	7.54e-2%
3	1284	3.24e-2%	2.13e-3%
4	1364	2.56e-3%	1.55e-4%

https://doi.org/10.4208/cicp.230815.090516a Published online by Cambridge University Press

Table 7: Two initial basis. Left: $tol=10^{-3}$. Middle: $tol=10^{-4}$. Right: $tol=10^{-5}$.

m	DOF	e_a	e_2
0	648	17.73%	3.58%
1	964	0.33%	1.85e-2%
2	972	0.30%	1.63e-2%

m	DOF	e_a	e_2
0	648	17.73%	3.58%
1	972	0.31%	1.80e-2%
2	1136	2.53e-2%	1.24e-3%

m	DOF	e_a	e_2
0	972	0.31%	1.80e-2%
1	1248	3.99e-3%	1.85e-4%
2	1276	2.49e-3%	1.19e-4%

Table 8: Three initial basis. Left: $tol=10^{-3}$. Middle: $tol=10^{-4}$. Right: $tol=10^{-5}$.

m	DOF	e_a	e_2
0	972	11.30%	1.72%
1	1248	0.50%	2.57e-2%
2	1276	0.24%	9.98e-3%

m	DOF	e_a	e_2
0	972	11.30%	1.72%
1	1296	0.45%	2.44e-2%
2	1436	2.60e-2%	9.70e-4%

m	DOF	e_a	e_2
0	1296	0.45%	2.44e-2%
1	1564	3.52e-3%	1.56e-4%
2	1576	2.49e-3%	1.04e-4%

adaptive algorithm. In Table 7 and Table 8, we show the errors for the last three iterations when using 2 and 3 initial basis functions respectively for tolerances 10^{-3}, 10^{-4} and 10^{-5}. We have the same observation that the energy errors have the same magnitude as the tolerances.

4.3 Adaptive online enrichment

In this section, we will show the performance for the online enrichment implementing it only for regions that have a cumulative residual that is θ fraction of the total residual. We consider the medium parameter shown in Fig. 4 (4 channels medium).

Assume that the local residuals are arranged such that

$$r_1 \geq r_2 \geq r_3 \geq \cdots,$$

where r_i is the norm of the local residual $\|R_i\|$. We only add the basis $\phi_1,\cdots,\phi_k$ for the coarse neighborhoods $\omega_1,\cdots,\omega_k$ such that k is the smallest integer with

$$\theta \sum_{i=1}^{N_c} r_i^2 \leq \sum_{i=1}^{k} r_i^2.$$

https://doi.org/10.4208/cicp.230815.090516a Published online by Cambridge University Press

Table 9: The results using cumulative errors with $\theta=0.5$, $tol=10^{-5}$ and 1 initial basis. Left: using energy norm based residual. Right: using L_2 norm based residual.

m	DOF	e_a	e_2
0	336	0.35%	3.80e-2%
1	352	0.27%	1.74e-2%
2	368	7.71e-3%	5.88e-4%
3	384	2.47e-3%	2.15e-4%
4	396	8.77e-4%	6.94e-5%

m	DOF	e_a	e_2
0	348	0.16%	5.19e-2%
1	368	0.10%	4.03e-2%
2	392	7.13e-2%	9.34e-3%
3	412	6.04e-3%	6.60e-4%
4	424	1.51e-3%	1.25e-4%

We will also consider two ways to compute the local residual r_i, one is based on L_2 norm and the other is based on an energy norm. For the L_2 norm based approach, we will compute $r_i=\|R_i\|$ where the norm is the L_2 norm. This is an inexpensive way to compute r_i. The energy norm based residual is to compute $r_i=\|R_i\|$ using an energy norm, which is defined in (3.6). In particular, we will solve a local problem to compute this norm. This requires a larger computational cost, but it provides a better solution.

In Table 9, we present the error for the last 5 iterations when using 1 initial basis functions with the tolerance 10^{-5} and $\theta=0.5$. We also present a comparison of using the L_2 based residual and the energy norm based residual. Comparing the result to the previous case, we can observe that this can use less number of basis functions to achieve a similar error. We also see that the energy norm based residual produces better solutions. In Fig. 5, we present the distribution of number of basis functions in coarse blocks, and see that the number of basis functions is larger near the channels (c.f. Fig. 4). Thus, online basis functions can be adaptively added in some regions using an error indicator.

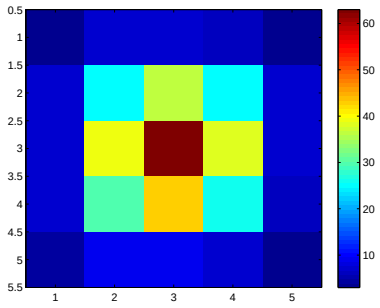


Figure 5: Distribution of number of basis functions in coarse blocks.

5 Conclusion

Though the use of offline basis functions is important for multiscale finite element methods, adding online basis functions in some regions can improve the convergence dra-

https://doi.org/10.4208/cicp.230815.090516a Published online by Cambridge University Press

matically. The construction of online basis functions for various applications and discretizations require a careful analysis. In particular, as we have shown earlier [9] for GMsFEM within continuous Galerkin framework that one needs a certain number of offline basis functions in order to guarantee that the online basis functions can result to a convergence independent of physical parameters. In this paper, we develop an online basis procedure for GMsDGM that can provide a convergence independent of the contrast and small scales. Because multiscale basis functions are discontinuous across coarse-grid boundaries, we construct a special offline space as well as online basis functions. We show that our construction will guarantee a convergence independent of the contrast and small scales if we select a certain number of offline basis functions based on a local spectral problem. Furthermore, we apply an adaptive procedure to add online basis functions in only some selected regions. Numerical results are presented to back up our theoretical findings.

Acknowledgments

This research is partially supported by the Hong Kong RGC General Research Fund (Project number: 400813). YE would like to thank the partial support from NSF 1620318, the U.S. Department of Energy Office of Science, Office of Advanced Scientific Computing Research, Applied Mathematics program under Award Number DE-FG02-13ER26165 and National Priorities Research Program grant 7-1482-1278 from the Qatar National Research Fund.

References

[1] A. Abdulle. Discontinuous Galerkin finite element heterogeneous multiscale method for elliptic problems with multiple scales. *Math. Comp.*, 81:687–713, 2012.
[2] A. Abdulle and Y. Bai. Adaptive reduced basis finite element heterogeneous multiscale method. *Comput. Methods Appl. Mech. Engrg.*, 257:203–220, 2013.
[3] T. Arbogast. Analysis of a two-scale, locally conservative subgrid upscaling for elliptic problems. *SIAM J. Numer. Anal.*, 42(2):576–598 (electronic), 2004.
[4] S. Brenner and L. Scott. *The Mathematical Theory of Finite Element Methods*. Springer-Verlag, New York, 2007.
[5] S. S. Chen, D. L. Donoho, and M. A. Saunders. Atomic decomposition by basis pursuit. *SIAM Rev.*, 43(1):129–159, 2001. Reprinted from SIAM J. Sci. Comput. **2**0 (1998), no. 1, 33–61 (electronic) [MR1639094 (99h:94013)].
[6] C.-C. Chu, I. G. Graham, and T.-Y. Hou. A new multiscale finite element method for high-contrast elliptic interface problems. *Math. Comp.*, 79(272):1915–1955, 2010.
[7] E. Chung and Y. Efendiev. Reduced-contrast approximations for high-contrast multiscale flow problems. *Multiscale Model. Simul.*, 8:1128–1153, 2010.
[8] E. Chung, Y. Efendiev, and R. Gibson. An energy-conserving discontinuous multiscale finite element method for the wave equation in heterogeneous media. *Advances in Adaptive Data Analysis*, 3:251–268, 2011.

https://doi.org/10.4208/cicp.230815.090516a Published online by Cambridge University Press

[9] E. Chung, Y. Efendiev, and T. Leung. Residual-driven online generalized multiscale finite element methods. submitted, arXiv:1501.04565.
[10] E. Chung, Y. Efendiev, and W. T. Leung. Generalized multiscale finite element method for wave propagation in heterogeneous media. *Multiscale Model. Simul*, 12:1691–1721, 2014.
[11] E. Chung, Y. Efendiev, and G. Li. An adaptive GMsFEM for high contrast flow problems. *J. Comput. Phys.*, 273:54–76, 2014.
[12] E. Chung and W. T. Leung. A sub-grid structure enhanced discontinuous galerkin method for multiscale diffusion and convection-diffusion problems. *Commun. Comput. Phys.*, 14:370–392, 2013.
[13] W. Dorfler. A convergent adaptive algorithm for poisson's equation. *SIAM J.Numer. Anal.*, 33:1106 – 1124, 1996.
[14] M. Drohmann, B. Haasdonk, and M. Ohlberger. Reduced basis approximation for nonlinear parametrized evolution equations based on empirical operator interpolation. *SIAM J. Sci. Comput.*, 34(2):A937–A969, 2012.
[15] L.J. Durlofsky. Numerical calculation of equivalent grid block permeability tensors for heterogeneous porous media. *Water Resour. Res.*, 27:699–708, 1991.
[16] W. E and B. Engquist. Heterogeneous multiscale methods. *Comm. Math. Sci.*, 1(1):87–132, 2003.
[17] Y. Efendiev and J. Galvis. A domain decomposition preconditioner for multiscale high-contrast problems. In Y. Huang, R. Kornhuber, O. Widlund, and J. Xu, editors, *Domain Decomposition Methods in Science and Engineering XIX*, volume 78 of *Lect. Notes in Comput. Science and Eng.*, pages 189–196. Springer-Verlag, 2011.
[18] Y. Efendiev, J. Galvis, and T. Hou. Generalized multiscale finite element methods. *Journal of Computational Physics*, 251:116–135, 2013.
[19] Y. Efendiev, J. Galvis, R. Lazarov, M. Moon, and M. Sarkis. Generalized multiscale finite element method. Symmetric interior penalty coupling. *J. Comput. Phys.*, 255:1–15, 2013.
[20] Y. Efendiev, J. Galvis, R. Lazarov, and J. Willems. Robust domain decomposition preconditioners for abstract symmetric positive definite bilinear forms. *ESAIM Math. Model. Numer. Anal.*, 46(5):1175–1199, 2012.
[21] Y. Efendiev, J. Galvis, G. Li, and M. Presho. Generalized multiscale finite element methods. oversampling strategies. to appear in International Journal for Multiscale Computational Engineering.
[22] Y. Efendiev, J. Galvis, and X.H. Wu. Multiscale finite element methods for high-contrast problems using local spectral basis functions. *Journal of Computational Physics*, 230:937–955, 2011.
[23] Y. Efendiev and T. Hou. *Multiscale Finite Element Methods: Theory and Applications*, volume 4 of *Surveys and Tutorials in the Applied Mathematical Sciences*. Springer, New York, 2009.
[24] Y. Efendiev, T. Hou, and V. Ginting. Multiscale finite element methods for nonlinear problems and their applications. *Comm. Math. Sci.*, 2:553–589, 2004.
[25] D. Elfverson, E. H. Georgoulis, and A. Malqvist. An adaptive discontinuous Galerkin multiscale method for elliptic problems. *Multiscale Model. Simul.*, 11:747–765, 2013.
[26] D. Elfverson, E. H. Georgoulis, A. Malqvist, and D. Peterseim. Convergence of a discontinuous Galerkin multiscale method. *SIAM J. Numer. Anal.*, 51:3351–3372, 2013.
[27] J. Galvis and Y. Efendiev. Domain decomposition preconditioners for multiscale flows in high contrast media. reduced dimension coarse spaces. *SIAM J. Multiscale Modeling and Simulation*, 8:1621–1644, 2010.
[28] K. Gao, E. Chung, R. Gibson, S. Fu, and Y. Efendiev. A numerical homogeneization method

https://doi.org/10.4208/cicp.230815.090516a Published online by Cambridge University Press

for heterogenous, anisotropic elastic media based on multiscale theory. *Geophysics*, 80:D385–D401, 2015.

[29] M. Ghommem, M. Presho, V. M. Calo, and Y. Efendiev. Mode decomposition methods for flows in high-contrast porous media. global-local approach. *Journal of Computational Physics, Vol. 253.*, pages 226–238.

[30] P. Henning, M. Ohlberger, and B. Schweizer. An adaptive multiscale finite element method. *Multiscale Model. Simul.*, 12:1078–1107, 2014.

[31] T. Hou and X.H. Wu. A multiscale finite element method for elliptic problems in composite materials and porous media. *J. Comput. Phys.*, 134:169–189, 1997.

[32] D. B. P. Huynh, D. J. Knezevic, and A. T. Patera. A static condensation reduced basis element method: approximation and *a posteriori* error estimation. *ESAIM Math. Model. Numer. Anal.*, 47(1):213–251, 2013.

[33] A. Malqvist and D. Peterseim. Localization of elliptic multiscale problems. *Math. Comp.*, 83:2583–2603, 2014.

[34] K. Mekchay and R. H. Nochetto. Convergence of adaptive finite element method for general second order elliptic PDEs. *SIAM J. Numer. Anal.*, 43:1803–1827, 2005.

[35] N. C. Nguyen, G. Rozza, D. B. P. Huynh, and A. T. Patera. Reduced basis approximation and a posteriori error estimation for parametrized parabolic PDEs: application to real-time Bayesian parameter estimation. In *Large-scale inverse problems and quantification of uncertainty*, Wiley Ser. Comput. Stat., pages 151–177. Wiley, Chichester, 2011.

[36] M. Ohlberger and F. Schindler. Error control for the localized reduced basis multi-scale method with adaptive on-line enrichment. *arXiv:1501.05202*.

[37] B. Riviere. *Discontinuous Galerkin Methods For Solving Elliptic And parabolic Equations: Theory and Implementation*. SIAM, 2008.

[38] T. Tonn, K. Urban, and S. Volkwein. Comparison of the reduced-basis and POD *a posteriori* error estimators for an elliptic linear-quadratic optimal control problem. *Math. Comput. Model. Dyn. Syst.*, 17(4):355–369, 2011.

[39] X.H. Wu, Y. Efendiev, and T.Y. Hou. Analysis of upscaling absolute permeability. *Discrete and Continuous Dynamical Systems, Series B.*, 2:158–204, 2002.

https://doi.org/10.4208/cicp.230815.090516a Published online by Cambridge University Press